CHALLENGES IN EUROPEAN AEROSPACE
5TH CEAS AIR & SPACE CONFERENCE

CEAS

Numerical and Experimental Investigations on Subsonic Air Intakes with Serpentine Ducts for UAV Configurations

Thomas M. Berens
AIRBUS Defence and Space GmbH
Expert Aerodynamic Propulsion Integration and Internal Aerodynamics
Rechliner Straße, 85077 Manching, Germany
thomas.berens@airbus.com

Anne-Laure Delot (ONERA – The French Aerospace Lab)
Magnus Tormalm (FOI Swedish Defence Research Agency)
Luis-Pablo Ruiz-Calavera and David-Ernesto Funes-Sebastian (AIRBUS Defence and Space)
Martin Rein (DLR, German Aerospace Center)
Michael Säterskog (SAAB AB, Aeronautics)
Nicola Ceresola (ALENIA Aermacchi)

ABSTRACT

Aerodynamic integration of diverterless air intakes with increasingly compact serpentine shaping and the optimization of their performance as well as engine/intake compatibility are challenging tasks for innovative design of advanced unmanned aerial vehicles (UAVs) featuring superior combat or reconnaissance abilities. Within the Aerodynamics Action Group AG-46 "Highly Integrated Subsonic Air Intakes" of the Group for Aeronautical Research and Technology in Europe (GARTEUR) various technological aspects were investigated in order to advance intake design solutions.
By applying modern hybrid Computational Fluid Dynamics (CFD) methods flow simulations were carried out for the EIKON UAV configuration which was previously designed and wind tunnel tested at FOI in Sweden. A major objective was to assess the capability of hybrid methods for the analysis of unsteady phenomena of serpentine air intakes and the accuracy levels of the computations. Numerical results for a variety of wind tunnel conditions were compared with Reynolds-Averaged Navier-Stokes (RANS) and unsteady RANS (URANS) data as well as experimental results. The time evolutions of distortion coefficients (e.g. DC60) at the aerodynamic interface plane (AIP) very well demonstrate the highly turbulent flow in the separated region downstream of the S-duct and allow the comparison of the dynamic intake distortion behavior with steady-state performance as well as experimental data, revealing an improved prediction of the time-averaged DC60 value with hybrid methods.
A numerical study on intake lip shaping was conducted allowing an improved assessment of the sources of the aerodynamic forces. The impact of boundary layer ingestion versus boundary layer diversion was investigated in a trade-off study. Eliminating the boundary layer resulted in improved total pressure recoveries at the intake throat by approximately 2%. Internal passive flow control was studied by employing numerical models for the simulation of vortex generators in the intake duct, and active flow control was researched by applying devices in form of micro-jets. Results were compared with experimental data. At DLR in Göttingen experiments with a generic high aspect ratio diverterless intake model were performed in the cryogenic blowdown wind tunnel DNW-KRG with the goal to contribute to a better understanding and correlation of installed performance predictions of highly integrated innovative intake designs. In a parametric study the combined effects of boundary layer ingestion and an S-shaped intake diffuser on total pressure recovery and dynamic distortion at the engine face were investigated as a function of Mach number, Reynolds number, boundary layer thickness and intake mass flow ratio.

NOMENCLATURE

A_c	intake capture area
A_0	cross section of captured stream tube at infinity
A_0/A_c	mass flow ratio (MFR), area ratio of captured stream tube
DC60	circumferential distortion parameter
M, Ma, Mach	Mach number
p	pressure
pr, PRA, pra	time-averaged static pressure/total pressure at infinity
MF, Q	mass flow
Q	dynamic pressure
qr	time-averaged dynamic pressure/total pressure at infinity
Re	Reynolds number
T	temperature, time period
t, tot	total state
v	velocity
x, y, z	coordinates in reference coordinate system
α, AoA	angle of attack
β, AoS	angle of sideslip
Δt	time step size
∞	state at infinity

AD/AG	GARTEUR Aerodynamics (AD) Action Group (AG)
AIP	Aerodynamic Interface Plane
CDI	Circumferential Distortion Index
ETA, PR	Total pressure recovery
RDI	Radial Distortion Index
S-A	Spalart-Allmaras (turbulence model)
VG	Vortex Generator
ZDES	Zonal Detached Eddy Simulation

1 INTRODUCTION

Advanced subsonic unmanned aerial vehicle designs require a high level of propulsion integration with increasingly compact shaping at the expense of increased aerodynamic complexity. In order to meet configurational requirements, innovative diverterless intake designs with optimized entry shaping and sophisticated serpentine duct layout are primary goals in the overall development process [1-3]. These design challenges, however, can generate intake flow characteristics, which can adversely impact the aerodynamic performance of the intake and the engine/intake compatibility. Unsteady flow physics like separation and reattachment as well as preentry and internal flow control implies an advanced degree of detailed understanding of the highly three-dimensional flow during the early design process. Installed thrust, range, and weight as additional key factors strongly relate to all these design requirements. Competitive aspects demand reduced development costs and short delivery times and thus are also main drivers within the UAV design process. Enhanced knowledge of the flow physics involved in complex innovative intake design can lead to improved methodologies for controlling these internal flows. In order to reduce costly wind tunnel experiments during the development phase of aerial vehicles the ability to accurately predict the aerodynamic performance of highly integrated intakes is of great importance.

The most promising simulation methods for time-accurate flow phenomena with high turbulence levels in an industrial environment are hybrid methods combining the inexpensive RANS (Reynolds-Averaged Navier-Stokes) and the accurate LES (Large Eddy Simulation) techniques. In particular, the Detached Eddy Simulation (DES) method [4] has received increasing attention over the past few years.

The major objective of the Aerodynamics Action Group AD/AG-46 "Highly Integrated Subsonic Air Intakes" of GARTEUR [5] (Group for Aeronautical Research and Technology in EURope) was to apply such methods at the forefront of innovative subsonic intake design and to evaluate their capabilities to accurately simulate unsteady internal flow fields. A comprehensive set of experimental data for highly integrated subsonic air intakes had been identified to validate unsteady numerical simulations in this field of research. Further areas of research within GARTEUR AD/AG-46 were computational predictions and experimental studies of dynamic intake distortion in complex flow fields due to S-shaped compactness of intake integration, flow separation effects due to challenging intake entry design, intake entry shaping, intake internal flow control, as well as boundary layer control and diversion for diverterless intakes.

Partners in the international collaboration of GARTEUR AD/AG-46 were AIRBUS Defence and Space (Germany, formerly CASSIDIAN, Chair, and Spain, formerly AIRBUS Military), ONERA (France, Vice-Chair), FOI (Sweden), SAAB (Sweden), DLR (Germany), Alenia Aermacchi (Italy), and MBDA (France). The results of all investigations are comprehensively documented in the AD/AG-46 final report [6]. The current paper gives a general overview of the research work performed and represents a condensed version of reference [7]. Further details about the results of specific objectives are documented in individual publications [8-11]. The GARTEUR Aerodynamics Action Group AD/AG-46 is the continuation of AD/AG-43 "Application of CFD to High Offset Intake Diffusers," [12-14], where numerical simulations were performed for an S-shaped diffuser and compared with experimental test data.

2 THE TEST UAV CONFIGURATION AND EXPERIMENTAL DATA

The geometry of a UAV (EIKON) with a double curved or serpentine intake duct, which was designed [15-16] and wind tunnel tested [17] at FOI, serves as a basis for the numerical simulations of steady and unsteady internal flow in subsonic air intakes. The EIKON features a delta/diamond wing planform with a 55° leading edge sweep and a 35° trailing edge sweep. The intended design of this UAV was for high subsonic flight at low altitude with a full scale wing span of 8 m. **Figure 1** shows the EIKON intake wind tunnel model in the T1500 Transonic Wind Tunnel. The model scale was fixed to 1:4.33 based on the available measuring rake for the aerodynamic interface plane (AIP) with total pressure probes, swirl probes, and Kulites®, as illustrated in **Figure 2**. In order to fit the model into the 1.5m x 1.5m test section of the pressurized T1500 wind tunnel, the wings had to be truncated. The span of the truncated intake model was 0.7 m, and the forebody length up to the throat station was approximately 0.5 m. The aft part of the model was simplified with a straight fairing to cover the installation.

Figure 1: EIKON UAV intake model in the T1500 Transonic Wind Tunnel.

2.1 The Intake Duct Geometry and Instrumentation of the UAV Configuration

The serpentine duct of the EIKON configuration has a length of 2.5 AIP diameters (**Figure 3**). The center line as well as the change of cross section along the center line are defined by combining trigonometric functions, with the throat having a kidney-shaped cross section. The diffuser offset prevents the direct line-of-sight onto the engine face at zero degrees elevation. The cowl of the intake features a W-type pattern with sharp lips, where the lips are aligned with the four major directions of the wing edges in the horizontal plane. Flow through the intake diffuser was achieved with an ejector system mounted inside the closed-loop wind tunnel.

The wind tunnel model was equipped with a measuring cell featuring a rake (diameter 154.2 mm) with 16 arms, each fitted with five total pressure probes located in an area-weighted radial position and one extra probe in the center on an extended arm (see Figure 2). Two radial locations (second and fourth ring) were additionally equipped with probes for swirl measurements. Eight Kulite® pressure transducers for recording of dynamic total pressures were positioned in the circumferential direction on separate arms between every second total pressure arm at the third ring radial location. Static pressures were measured at the duct wall in the rake plane as well as at 58 ports along the upper, lower, and side walls of the intake diffuser (Figure 3). The experimental data also comprise 24 static wall pressure ports upstream of the duct on the forebody surface.

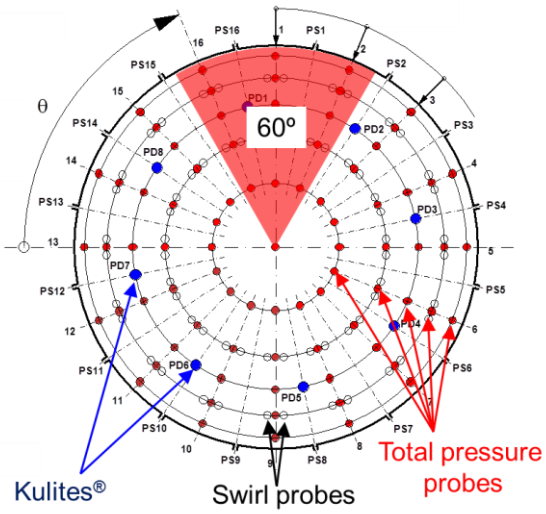

Figure 3: Test rake at the aerodynamic interface plane (AIP) with total pressure probes, swirl probes and Kulites®.

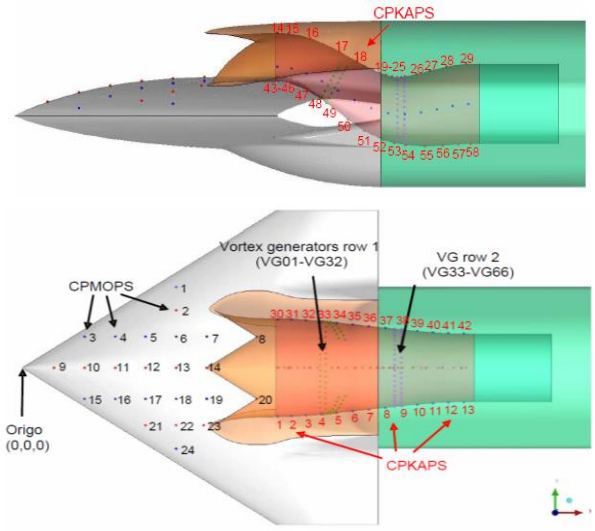

Figure 2: Top and side views of the wind tunnel model with the static pressure ports on the forebody and the duct walls.

2.2 Experimental Data for Comparison with Numerical Results

For computational investigations within GARTEUR AD/AG-46, eight different operating conditions for the EIKON intake model were selected as test cases. They cover variations in Mach number, Reynolds number, angle of attack, angle of side slip and mass flow. The proposed test cases are specified in **Table 1**. For the full scale configuration, a design mass flow of 62.5 kg/s (at Mach 0.85, sea level) was considered to be 100%. The experimental Reynolds number is calculated from wind tunnel free stream

conditions and is based on the intake AIP diameter of 0.1524 m. The mass flow rate was controlled by an ejector system, which automatically stabilized the flow to a prescribed corrected mass flow value. The mass flow was measured with a venturi nozzle, calibrated prior to the tests.

Case	M	Re (·10^6)	AoA, deg	AoS, deg	Mass flow rate, %	Comment
1	0.85	3	0	0	100	Baseline design case
2	0.85	7	0	0	100	Highest Re available
3	0.80	3	0	0	100	Nominal case at Mach 0.8
4	0.80	3	10	0	100	High AoA
5	0.80	3	0	0	50	Effects of mass flow variation
6	0.80	3	0	-10	100	High sideslip, lip vortex
7	0.60	3	0	0	100	Mach number variation
8	0.80	3	0	0	75	Effects of mass flow variation

Table 1: Test cases of the UAV wind tunnel tests applied for computational investigations.

2.3 Grid Generation

All partners of AD/AG-46 generated their own computational grids according to the requirements of the codes applied. While ONERA and AIRBUS Defence and Space Spain used structured grids for their computations, all other partners generated unstructured meshes. **Table 2** provides a summary of the main grid characteristics. More details about the meshes are given in [6] and [7].

Partner	Span	Nodes	Prisms	Tetrahedras	Hexas	Duct nodes surf/inner	Boundary layers	First cell height (m)
FOI	Full	13 516 054	21 911 898	14 174 702	n/a	79 368/4 873 830	50	1.0e-6
SAAB	Full	9 500 000	16 800 000	3 900 000	n/a	81 000/3 660 000	40	1.0e-6
AIRBUS D&S G	Full (1)	39 207 244	21 301 534	169 929 282	n/a	not avail.	36	2.5e-6
AIRBUS D&S G	Full (2)	39 408 074	21 572 904	170 283 318	n/a	not avail.	36	2.5e-6
AIRBUS D&S E	Half (3)	2 983 855	n/a	n/a	2 685 785	not avail.	30 (model)	2.0e-6
AIRBUS D&S E	Half (4)	1 795 471	n/a	n/a	1 593 257	not avail.	30 (model)	2.0e-6
ONERA	Full	43 767 574	n/a	n/a	40 267 990	not avail.	30	1.3E-6
Alenia (adapted)	Full	7 710 234	9 682 542	16 182 148	not avail.	not avail.	21	5.0E-6

(1) Sharp intake cowl, (2) Round intake cowl, (3) Free onset flow, (4) T1500 Wind Tunnel

Table 2: Summary of main characteristic values for computational meshes.

2.4 Numerical Methods and Boundary Conditions

A brief description of the numerical methods applied by all AD/AG-46 partners and of the corresponding boundary conditions is given below. Further details are provided in [6-10].

All FOI computations were performed with the flow solver EDGE [18]. The turbulence model selected for both the RANS and URANS computations was the Wallin-Johansson [19] Explicit Algebraic Reynolds Stress Model (EARSM) with the Hellsten k-ω model. All cases were calculated as fully turbulent. A mass flow condition was used at the duct outflow boundary. The time accurate URANS simulations used the same settings as the RANS simulations except for the implicit dual-time stepping setup with a global time step of 2.0×10^{-5} s. The number of maximum inner iterations was set to 40. For the time accurate approach, hybrid RANS/LES methods based on the Spalart-Allmaras turbulence model were selected.

The SAAB CFD calculations were performed with the FOI developed flow solver EDGE [18]. The differences between the FOI and Saab calculations are in the grid resolution described in Table 2, and in the different turbulence models applied. For the RANS and URANS calculations, a Menter SST k-ω model [20] was used, and for the hybrid RANS/LES calculations an algebraic hybrid HYB0 model by Peng [21] was applied. The time step was 5.0×10^{-6} s for the hybrid calculations. An upper limit of 150 inner iterations was applied to achieve a two orders of residual reduction for each time step. In total 37000 time steps were calculated to achieve approximately 80 duct passages.

ONERA performed RANS and ZDES (Zonal Detached Eddy Simulation) calculations with the FLU3M in-house code on a multi-block structured grid. ZDES has first been proposed in [24], and a generalized formulation including implementation details has recently been proposed in [25] and [26]. In order to achieve the experimental intake mass flow, ONERA added a circular pipe followed by a convergent-divergent nozzle at the end of the diffuser and set an inactive boundary condition in order to reach sonic conditions at the nozzle throat. The supersonic flow in the divergent part prevents the outlet boundary condition from influencing the flow at the AIP. The throat is adjusted to reach the desired mass flow. A physical time step size of $\Delta t = 2.5 \times 10^{-7}$ s with 5 subiterations was applied for the ZDES computation.

AIRBUS Defence and Space Germany applied the finite-volume DLR-TAU-Navier-Stokes Code [22] for the DES flow field computations. A Spalart-Allmaras turbulence model variant (DES S-A) was used in the present work. The switch between RANS and LES modes is based on a modified definition of the characteristic length scale in the Spalart-Allmaras turbulence model, depending on the distance from the wall and the largest edge length of the local grid cell. As outflow boundary condition for the intake duct exit the value of the experimental duct mass flow rate was set for the specific test cases. A physical time step size of $\Delta t = 2.0 \times 10^{-5}$ s was applied with 40 subiterations.

AIRBUS Defence and Space Spain calculations were performed using ANSYS® CFX™ [23], a commercial CFD code. CFX is an implicit, pressure based, node centered, control volume solver. The turbulence model selected is the k-ω SST with the CFX automatic wall functions formulation. Engine air mass flow is controlled by means of a static pressure outlet condition, set to match the experimental mass flow rate within an error lower than 0.1%. In free flight conditions, flow magnitudes (air speed and direction, static temperature, and static pressure) are imposed in the farfield, equal to the experimental test conditions. Wind tunnel slots were simulated using an opening boundary condition allowing inflow and outflow.

ALENIA Aermacchi conducted the computations with the in-house code UNS3D. The solution algorithm is based on a finite volume, node centered scheme operating on an unstructured grid. The artificial dissipation model is derived from the nonlinear scheme of Jameson. The Wallin-Johansson [19] Explicit Algebraic Reynolds Stress Model (EARSM) was used with the Hellsten k-ω model as the basic RANS procedure. URANS computations were performed using a time step of 2.0×10^{-4} s. For DES simulations, the k-ω-EARSM model was applied in RANS regions. A time step size of 5.0×10^{-5} s was used with a limit of 100 subiterations at each step.

3 NUMERICAL RESULTS FOR THE EIKON UAV WIND TUNNEL MODEL

3.1 CFD Computations for the EIKON Wind Tunnel Model Configuration

Navier-Stokes computations were carried out for the EIKON UAV wind tunnel model (Figure 1) and eight test cases from experimental investigations (Table 1) with different turbulence models. While each partner of GARTEUR AD/AG-46 chose specific test cases from Table 1, all partners computed test case 1 (EIKON baseline design case) for benchmarking purposes.
DES calculations were performed for the wind tunnel conditions, and unsteady total pressures at the probe positions of the measuring rake (see Figure 2) from the experiments were recorded. Static pressures at the locations of the wind tunnel model's pressure tabs on the forebody and in the diffuser were gathered. For comparison with the hybrid simulations, RANS and URANS computations were conducted. The numerical results were compared with available experimental data.
Detailed results from the RANS, URANS, and DES computations are provided in references [7] and [8]. In the current paper a comprehensive summary of the results is presented.

Figure 4 displays ONERA ZDES results for test case 1. The unsteady character of the intake flow field with two vortices at the bottom and massive flow separation at the top side of the duct is clearly revealed by the Schlieren-like visualizations of the instantaneous flow field in the symmetry plane of the intake model as well as in the AIP. The separated flow region has much in common with a two-dimensional backward facing step flow with respect to the shear layer instability process [27].

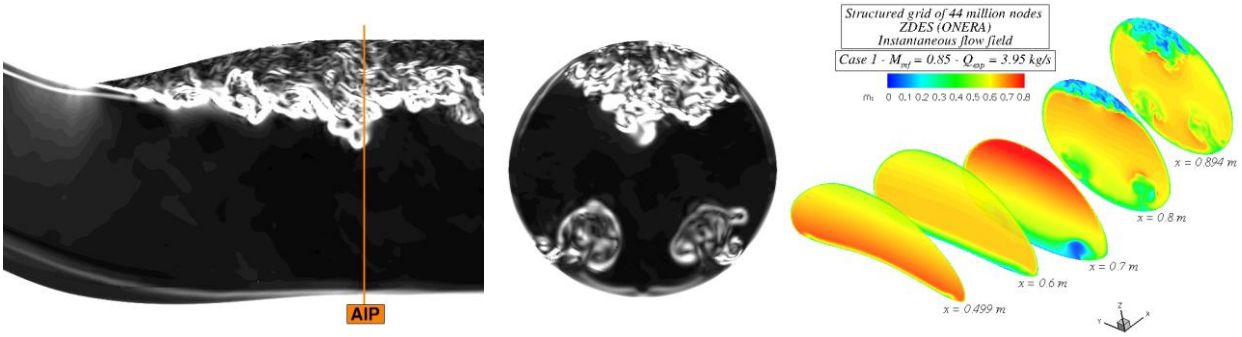

Figure 4: ONERA ZDES results for test case 1: Schlieren-like visualization of instantaneous flow field in symmetry plane (left) and in AIP (center), and Mach number distributions in various x=const cross sections in the intake duct (right).

ALENIA Aermacchi's numerical results for test case 1 are shown in **Figure 5** with Mach number and total pressure distributions in the AIP. The separation region near the upper surface and the two streamwise vortices in the lower part of the duct are evident in the RANS solutions. Several unsteady flow structures are resolved by applying the DES-EARSM model. All DES computations were carried out for a total time of 0.1 s.

The very dynamic character of the intake flow field is best revealed by the various distortion parameters (circumferential and radial distortion indices, DC60 distortion coefficient) for which the computational results are compared with the experimental data and are discussed in detail in references [6], [7], and [8]. While RDI and DC60 results from ONERA RANS and ZDES simulations compare well with the experimental data, the instantaneous values of computed total pressure recovery are almost

systematically higher than the experimental values. The time-averaged value for the total pressure recovery, however, is 1% higher than the experimental one, while the computed CDI value is systematically underestimated compared to the experiment.

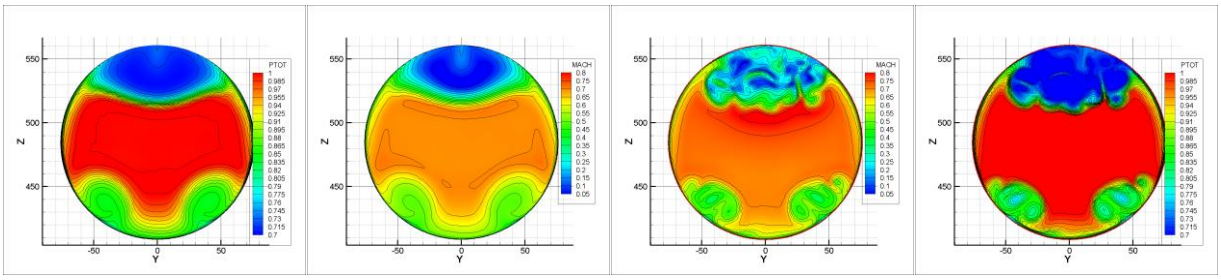

Figure 5: ALENIA Aermacchi results for test case 1: from left to right, pressure recovery and Mach number in AIP (RANS), Mach number and pressure recovery in AIP (DES).

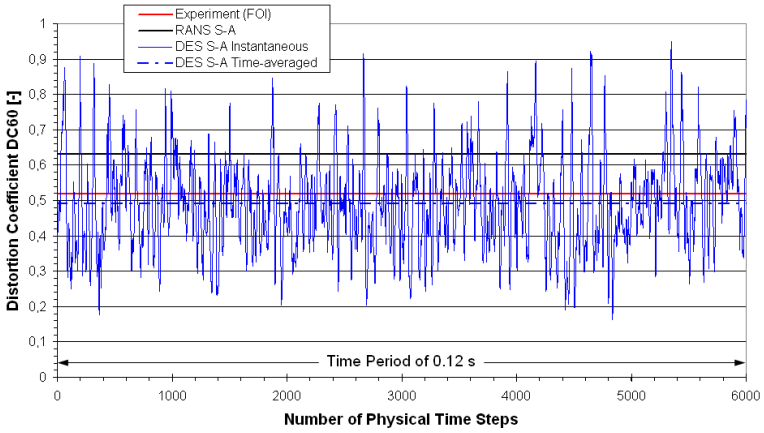

Figure 6: AIRBUS Defence and Space distortion coefficients DC60 for test case 3 (sharp intake cowl, Mach 0.80, mass flow 3.97 kg/s), DES results vs. RANS S-A computations and FOI experimental measurements.

DC60 results versus time from AIRBUS Defence and Space Germany computations are presented exemplary for test case 3 in **Figure 6**. A comparison of time-averaged DC60 values from DES computations with experimental data demonstrates good agreement for test cases 1 [7] and 3 (Figure 6). Deviations for test cases 7 and 8 are about 0.06 and 0.08, respectively [7]. Except for test case 8 with the reduced duct mass flow rate, RANS results do not match the experimental values for DC60 very well [7]. Deviations between RANS and DES time-averaged results are generally in the order of 0.15 for the investigated test cases.

The calculation of the time-averaged DC60 values from the DES instantaneous solutions do not take the non-linear behavior of the fluctuating total pressures into account. By calculating the DC60 values from time-averaged total pressures in the AIP, a more accurate estimation of the time averaged DC60 could be expected. This method was exemplary tested for the hybrid RANS/LES computation of test case 1 by SAAB [7], which led to a time-averaged value for DC60 of 0.533 close to the experimental value of 0.529.

All numerical solutions were primarily analyzed at the aerodynamic interface plane (AIP) with respect to overall performance such as total pressure recovery and distortion coefficients. Distortion descriptors (Rolls Royce Distortion Coefficient DC60, Circumferential Distortion Index CDI, Radial Distortion Index RDI) and swirl descriptors (Swirl Coefficient SC60) were taken from references [28] and [29].

For all partners of GARTEUR AD/AG-46, the numerical results in the aerodynamic interface plane (AIP) are summarized in **Table 3**. For the evaluation of the parameters from the computational data the tools provided by AIRBUS Defence and Space Spain were applied. Most FOI data in Table 3 were evaluated as mean values of the final 500 iterations. The only exception is the FOI swirl parameter which has been analyzed using the mean solution. The experimental swirl probes cannot detect the high time-dependent swirl values, which sometimes are larger than the calibration maximum of 30 degrees. The comparison of the CFD swirl with the experimental data is also questionable due to reverse flow in the upper AIP region, and this region determines the value of the swirl descriptor SC60. The time-accurate DES S-A simulations indicate large and rapid fluctuations. Therefore, the experimental values agree much better with the mean solutions (Table 3).

The experimental data included time traces from eight high response total pressure transducers. Their locations are shown in Figure 2. In order to evaluate the dynamic characteristics of the calculated total pressures in the AIP, a comparison of the root mean square (RMS) values of the dynamic total pressures was performed [7]. Large areas of separations exist with very high turbulent intensities (high RMS values), which have been well identified in the simulations.

Figure 7, as an illustration of the listed results for test case 1 in Table 3, shows the total pressure recoveries (ETA) in the AIP as well as the DC60 parameters from different simulation methods and the comparison with the experimental values. While computational results for the total pressure recoveries do not show clear preferences for the application of specific simulation methods, experimental DC60 values are best matched by DES results. The discrepancies between numerical results and experiment are mainly due to the more or less accurate prediction of the low total pressure region (in terms of level and spanwise extension) in the upper portion of the AIP, resulting from the upstream flow separation. This low total pressure core is responsible for the high flow distortion extremely difficult to accurately predict by computations. A benefit of performing time-accurate RANS (i.e. URANS) computations instead of steady state RANS calculations cannot be identified from Figure 7. RANS and URANS computations gave very similar results for the total pressure recoveries as well as the distortion coefficients and delivered higher DC60 values than DES results, whereas hybrid RANS/LES results better match the experimental data. The results prove advantages of using advanced time-accurate methods such as DES to predict instantaneous flow field parameters required to accompany the design process of highly integrated subsonic air intakes, especially with respect to dynamic intake distortion and thus engine/intake compatibility, even if capabilities still need to be improved to reach accuracy levels required for project-oriented applications.

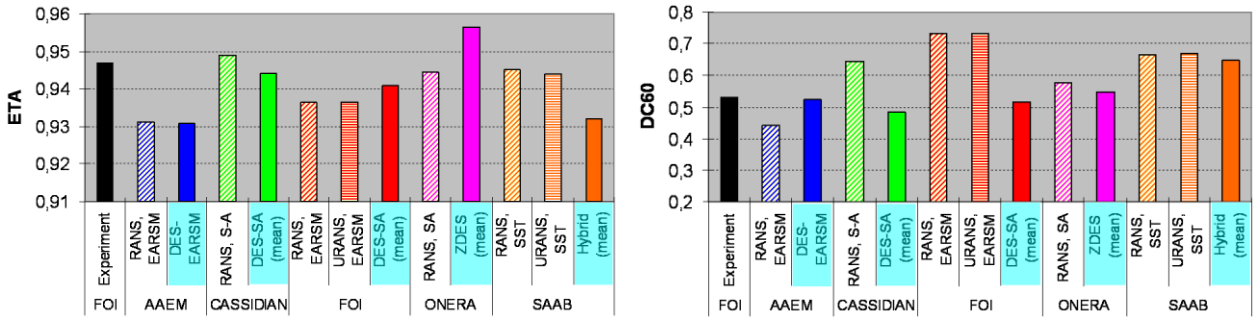

Figure 7: Total pressure recoveries (ETA) in the AIP and distortion coefficients DC60 from different simulation methods and comparison with experimental values (see also Table 3).

Test Case	Partner	Method	PR	DC60	CDI	RDI	SC60	$\dot{m}$ (kg/s)	Remarks
1	FOI	Experiment	0.9470	0.5290	0.1494	0.0273	16.06	3.953	
	FOI	RANS, EARSM	0.9364	0.7339	0.1484	0.0341	16.18	3.977	
	SAAB	RANS, SST	0.945	0.666	0.231	0.025	13.6	3.948	
	AIRBUS D&S E	RANS k-w SST	0.9439	0.6072	0.1340	0.0314	-	3.950	
	AIRBUS D&S G	RANS, S-A	0.9489	0.6446	0.1138	0.0268	-	3.953	
	ONERA	RANS, S-A	0.9445	0.5778	0.1341	0.0290	18.22	3.989	
	ALENIA	RANS, EARSM	0.9310	0.4400	0.1706	0.0586	-	3.953	
	MBDA	RANS S-A	0.947	0.5566	0.1192	0.0366	13.61	3.953	
	FOI	URANS, EARSM (mean)	0.9364	0.7334	0.1484	0.0342	15.94	3.977	
	SAAB	URANS, SST (mean)	0.944	0.668	0.229	0.023	13.5	3.950	
	FOI	DES S-A (mean)	0.9410	0.5168	0.1323	0.0345	17.33	3.972	
	AIRBUS D&S G	DES S-A (mean)	0.9441	0.4840	0.1147	0.0318	34.28	3.953	
	ALENIA	DES-EARSM	0.9309	0.5232	0.1852	0.0349	-	3.953	
	ONERA	ZDES	0.9563	0.5493	0.1202	0.0282	13.17	3.963	
	SAAB	Hybrid (mean)	0.932	0.649	0.215	0.028	26.6	3.922	
2	FOI	Experiment	0.9509	0.4910	0.1395	0.0280	18.86	9.561	
	FOI	RANS, EARSM	0.9459	0.6977	0.1435	0.0314	12.62	9.628	
	SAAB	RANS, SST	0.953	0.603	0.238	0.021	11.8	9.551	
	MBDA	RANS S-A	0.953	0.5155	0.1114	0.0364	12.63	9.561	
	FOI	URANS, EARSM (mean)	0.9473	0.6963	0.1393	0.0302	12.65	9.532	
	FOI	DES S-A (mean)	0.9451	0.5838	0.1324	0.0298	44.32	9.356	
3	FOI	Experiment	0.9481	0.5181	0.1465	0.0274	15.55	3.970	
	FOI	RANS, EARSM	0.9384	0.7292	0.1463	0.0347	15.30	3.995	
	SAAB	RANS, SST	0.947	0.659	0.229	0.024	13.4	3.965	
	AIRBUS D&S E	RANS k-w SST	0.9465	0.5982	0.1324	0.0321	-	3.968	
	AIRBUS D&S G	RANS, S-A	0.9520	0.6296	0.1149	0.0305	-	3.970	
	ALENIA	RANS, EARSM	0.9215	0.6542	0.1460	0.0549	-	3.970	
	MBDA	RANS S-A	0.950	0.5466	0.1165	0.0368	13.53	3.970	
	FOI	URANS, EARSM (mean)	0.9368	0.7301	0.1513	0.0361	15.21	4.039	
	FOI	DES S-A (mean)	0.9347	0.6225	0.1492	0.0361	30.74	3.984	
	AIRBUS D&S G	DES S-A (mean)	0.9460	0.4906	0.1128	0.0326	33.21	3.970	
	ALENIA	DES-EARSM (instant.)	0.9262	0.3357	0.1111	0.0604	-	3.970	
4	FOI	Experiment	0.9422	0.4943	0.1279	0.0363	15.70	3.955	
	FOI	RANS, EARSM	0.9334	0.6955	0.1426	0.0331	14.03	3.951	
	SAAB	RANS, SST	0.930	0.659	0.229	0.038	11.4	3.934	
	MBDA	RANS S-A	0.940	0.5340	0.1122	0.0328	14.35	3.955	
	FOI	URANS, EARSM (mean)	0.9262	0.6686	0.1447	0.0344	12.92	3.996	No conv.
	FOI	DES S-A (mean)	0.9330	0.5671	0.1427	0.0516	26.14	4.124	

Table 3: Main results for the total pressure recoveries and the distortion coefficients in the aerodynamic interface plane (AIP).

Test Case	Partner	Method	PR	DC60	CDI	RDI	SC60	$\dot{m}$ (kg/s)	Remarks
5	FOI	Experiment	0.9422	0.2403	0.0116	0.0082	6.25	1.971	
	FOI	RANS, EARSM	0.9362	0.7072	0.0473	0.0141	16.55	1.989	
	SAAB	RANS, SST	-	-	-	-	-	-	No conv.
	AIRBUS D&S G	RANS, S-A	-	-	-	-	-	-	No conv.
	FOI	URANS, EARSM (mean)	0.9303	0.8214	0.0285	0.0075	13.90	1.451	No conv.
	FOI	DES S-A (mean)	0.9201	0.6189	0.0106	0.0056	62.67	0.742	No conv.
	AIRBUS D&S G	DES S-A (mean)	0.9703	0.4573	0.0243	0.0113	36.36	1.971	Bad conv.
6	FOI	Experiment	0.9432	0.4232	0.1052	0.0246	19.91	4.103	
	FOI	RANS, EARSM	0.9387	0.6888	0.1368	0.0253	13.97	4.109	
	SAAB	RANS, SST	0.943	0.548	0.238	0.025	13.4	4.112	
	ALENIA	RANS-EARSM	0.8862	0.4086	0.1239	0.0303	-	4.103	
	MBDA	RANS S-A	0.943	0.5589	0.0742	0.0347	9.86	4.103	
	FOI	URANS, EARSM (mean)	0.9445	0.6829	0.1208	0.0219	15.17	3.942	
	FOI	DES S-A (mean)	0.9511	0.4363	0.0974	0.0205	22.34	3.910	
	ALENIA	DES-EARSM (instant.)	0.8800	0.4625	0.1582	0.0332	-	4.103	
7	FOI	Experiment	0.9557	0.4870	0.1284	0.0272	15.33	3.981	
	FOI	RANS, EARSM	0.9510	0.6926	0.1342	0.0348	12.38	4.011	
	SAAB	RANS, SST	0.959	0.586	0.222	0.029	11.5	3.978	
	AIRBUS D&S G	RANS, S-A	0.9625	0.5769	0.0984	0.0380	-	3,981	
	AIRBUS D&S E	RANS k-w SST	0.9589	0.5393	0.1171	0.0347	-	3.982	
	MBDA	RANS S-A	0.960	0.5204	0.1007	0.0367	11.11	3.981	
	AIRBUS D&S G	DES S-A (mean)	0.9598	0.4270	0.0941	0.0341	30.00	3.981	
8	FOI	Experiment	0.9593	0.5756	0.0696	0.0203	16.72	3.040	
	FOI	RANS, EARSM	0.9553	0.7345	0.0719	0.0209	21.53	3.051	
	SAAB	RANS, SST	0.960	0.688	0.182	0.011	15.3	3.036	
	AIRBUS D&S E	RANS k-w SST	0.9630	0.5242	0.0419	0.0160	-	3.041	
	MBDA	RANS S-A	0.962	0.5210	0.0582	0.0176	10.21	3.040	
	AIRBUS D&S G	RANS, S-A	0.9614	0.6167	0.0421	0.0132	-	3.040	
	AIRBUS D&S G	DES S-A (mean)	0.9576	0.4904	0.0641	0.0217	35,91	3.040	

Table 3 (continued): Main results for the total pressure recoveries and the distortion coefficients in the aerodynamic interface plane (AIP).

3.2 Wind Tunnel and Model Geometry Effects on CFD Results and Wind Tunnel Wall Interference on EIKON Experimental Tests

RANS k-ω SST calculations were performed by AIRBUS Defence and Space Spain for the EIKON model for test cases 1, 3, 7, and 8 with two different CFD models, in order to simulate free stream conditions and T1500 slotted test section conditions. Additionally, case 7 with an onset flow Mach number of 0.6 was also simulated with closed slots of the T1500 wind tunnel. The computational results for the total pressure recovery and the distortion coefficients are listed in **Table 4**.

Case	Partner	Method	PR	DC60	CDI	RDI	$\dot{m}$ (kg/s)
1	AIRBUS D&S E	RANS k-w SST, free flight	0.9439	0.6072	0.1340	0.0314	3.950
1	AIRBUS D&S E	RANS k-w SST, ventilated WT	0.9441	0.6066	0.1340	0.0316	3.951
3	AIRBUS D&S E	RANS k-w SST, free flight	0.9465	0.5982	0.1324	0.0321	3.968
3	AIRBUS D&S E	RANS k-w SST, ventilated WT	0.9467	0.5978	0.1324	0.0322	3.969
7	AIRBUS D&S E	RANS k-w SST, free flight	0.9589	0.5393	0.1171	0.0347	3.982
7	AIRBUS D&S E	RANS k-w SST, ventilated WT	0.9589	0.5394	0.1172	0.0348	3.982
7	AIRBUS D&S E	RANS k-w SST, closed WT	0.9578	0.5476	0.1186	0.0340	3.981
8	AIRBUS D&S E	RANS k-w SST, free flight	0.9630	0.5242	0.0419	0.0160	3.041
8	AIRBUS D&S E	RANS k-w SST, ventilated WT	0.9632	0.5234	0.0418	0.0161	3.041

Table 4: Total pressure recoveries and distortion coefficients in the AIP from RANS computations by Airbus Defence and Space Spain for free flight and ventilated wind tunnel conditions.

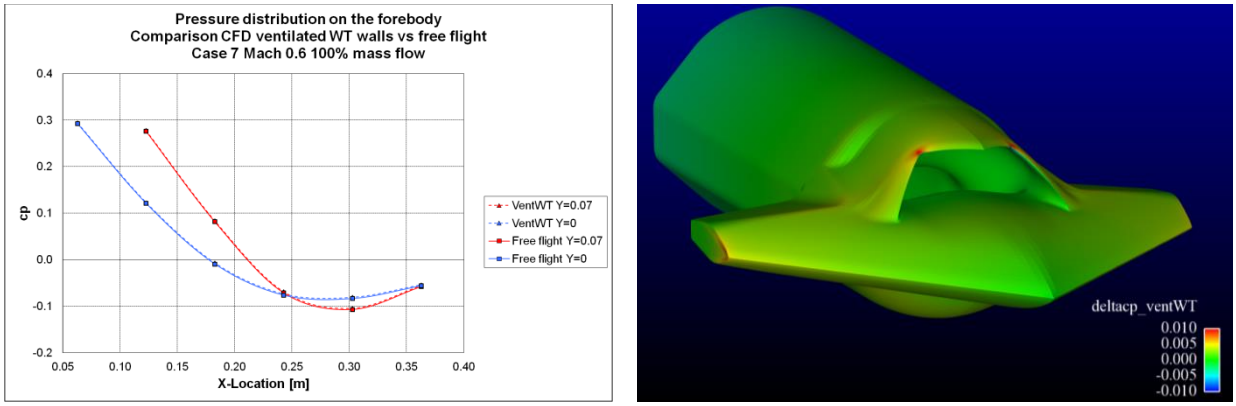

Figure 8: Numerical cp-distributions on the forebody in free flight and within the T1500 test section (left) and difference of cp-distribution on the model, within T1500 test section minus free flight (right), test case 7.

Figure 8 shows numerical results for the static pressure distributions on the forebody for free flight boundary conditions and for the slotted T1500 test section. Deviations of the pressure coefficients between these conditions are minimal, in the order of ΔCp = 0.01.

The difference between the numerical pressure distribution on the model surface calculated for test case 7 within the wind tunnel and in free flight conditions is also shown in Figure 8. Maximum interference is in the order of ΔCp = 0.01 only, and it is located at the corners of the W-shaped cowl on the external lips and on the leading edges of the truncated wing near the wing tips. Within the intake duct, wind tunnel wall interference has even smaller effects. AIP total pressure distributions based on the experimental AIP rake locations are practically identical, which is proven by the total pressure recoveries and distortion parameters listed in Table 4. Further details of these investigations are documented in [10], where also effects of closed wind tunnel slots are addressed, and comparisons are made between free stream and closed test section conditions.

Overall results lead to the conclusion that wind tunnel wall interference of the EIKON model within the T1500 test section is negligible. The ventilated walls of the T1500 wind tunnel practically eliminate the blockage of the model which would occur in a closed test section. According to these results, a comparison between the CFD results calculated with free stream boundary conditions and the experimental data for the UAV configuration is validated.

3.3 Numerical Study on Intake Lip Shaping

AIRBUS Defence and Space Germany performed a numerical study on intake lip shaping as a vital design parameter impacting the intake internal flow and aerodynamic performance. As alternative lip shaping to the current EIKON design, thickening of the cowl was performed while keeping the shape of the intake and the sweep angles of the W-cowls according to the original geometry. Emphasis was put on the aerodynamic forces produced by the original sharp cowl design and the modified round cowl. Further details are provided in references [6] and [7].

RANS computational results for intake performance and aerodynamic forces for the complete intake wind tunnel model at zero degrees angle of attack were compared for the reference configuration with sharp intake lips and the modified geometry with the round cowl. **Figure 9** and **Figure 10** show the drag coefficients for the complete model, as well as breakdowns for all individual parts of the model. The first column on the left side in these graphs (category "Complete_Model") shows the sum of all other individual parts in each case. The reference value for the force coefficients is the wing area of the scaled UAV with 3.416763 m^2. Color coding for all surfaces of the wind tunnel model facilitates the assignment of the forces to specific model parts.

The impact of the onset flow Mach number on drag coefficients is provided in Figure 9. The decreasing drag coefficients of the wing due to decreasing onset flow Mach numbers are quantified. Drag coefficients for the complete model with the round cowl at Mach numbers 0.6 and 0.8 are almost equal. The sharp cowl configuration leads to an increase of drag at Mach 0.6 due to increased forces at the engine face. The complete cowls themselves do not produce drag, since flow conditions at the external parts of the cowl produce suction.
For the investigated test cases at Mach numbers 0.85, 0.80, and 0.60, drag components due to the intake cowl itself are generally small compared to the other parts of the configuration. The intake cowl design, however, influences the aerodynamic performance of other parts of the UAV model (e.g. engine face at Mach 0.6). Lift coefficients for the complete model are distinctly influenced by the contribution of the intake cowl [7]. Lift components provided by the round cowl design are larger than for the sharp cowl due to lower pressure distributions at the rounded lip surfaces.

The impact of the engine air mass flow on drag coefficients is illustrated in Figure 10 for an onset flow Mach number of 0.8. For the complete model, decreasing mass flows result in decreasing drag forces. Drag components of the wing, however, are increasing. For decreasing mass flows the contributions of the intake cowl to the thrust forces are increasing due to improved flow conditions at the external parts of the intake cowl [7]. Comparing the influence of the sharp and round cowls results in increasing advantages for the round cowl with decreasing engine air mass flows.

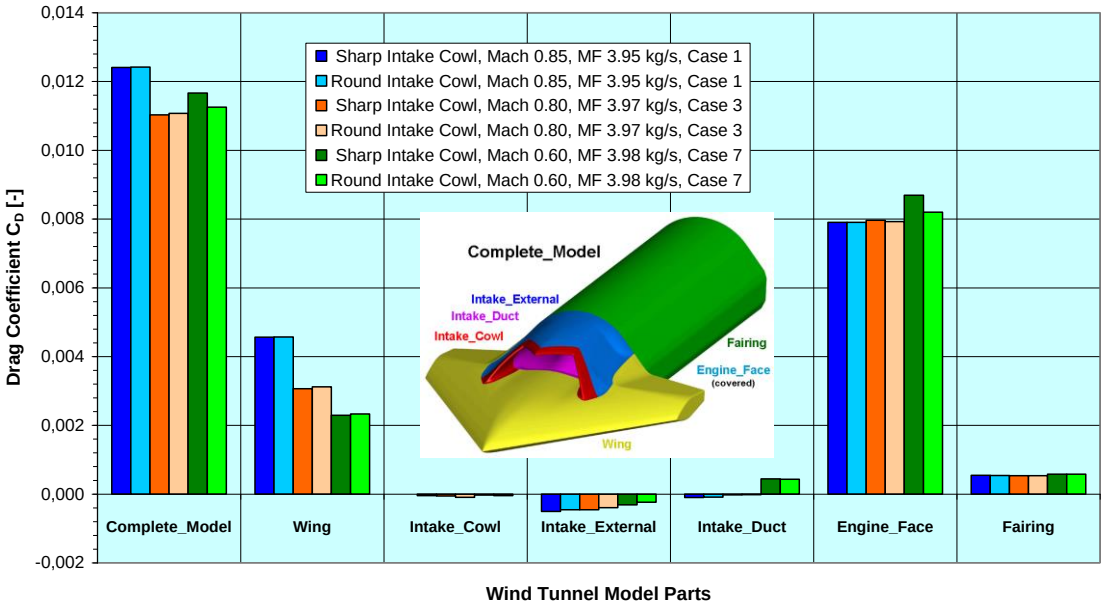

Figure 9: Impact of onset flow Mach number on drag coefficients for the complete wind tunnel model with original sharp intake cowl and modified round cowl (AIRBUS Defence and Space Germany RANS results).

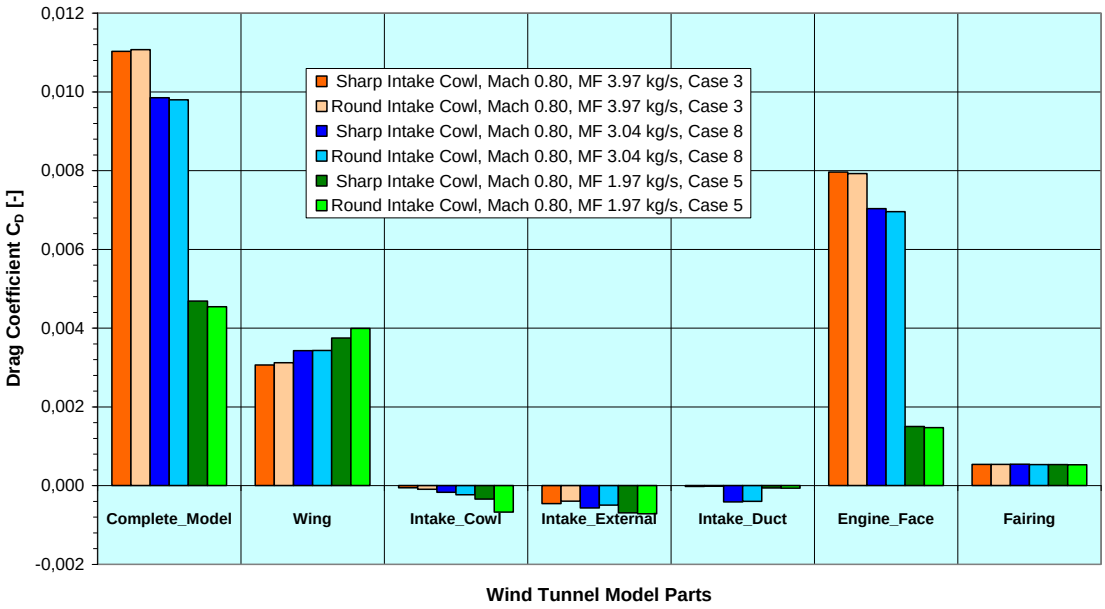

Figure 10: Impact of engine air mass flow on drag coefficients for the complete wind tunnel model with original sharp intake cowl and modified round cowl (AIRBUS Defence and Space Germany RANS results).

3.4 Boundary Layer Diversion versus Ingestion

The impact of boundary layer ingestion versus boundary layer diversion was investigated in a trade-off study by FOI. Computations were performed applying Euler boundary conditions at the forebody. When the boundary layer was removed, the total pressure losses decreased as expected and were quantified. Removing the boundary layer improved the recovery at the throat (**Figure 11**) by approximately 2%. Distortion in the AIP decreased. All results for the Euler forebody cases are summarized in **Table 5**. Listed are the total pressure recoveries and the distortion parameters. More detailed results are given in references [6] and [7].

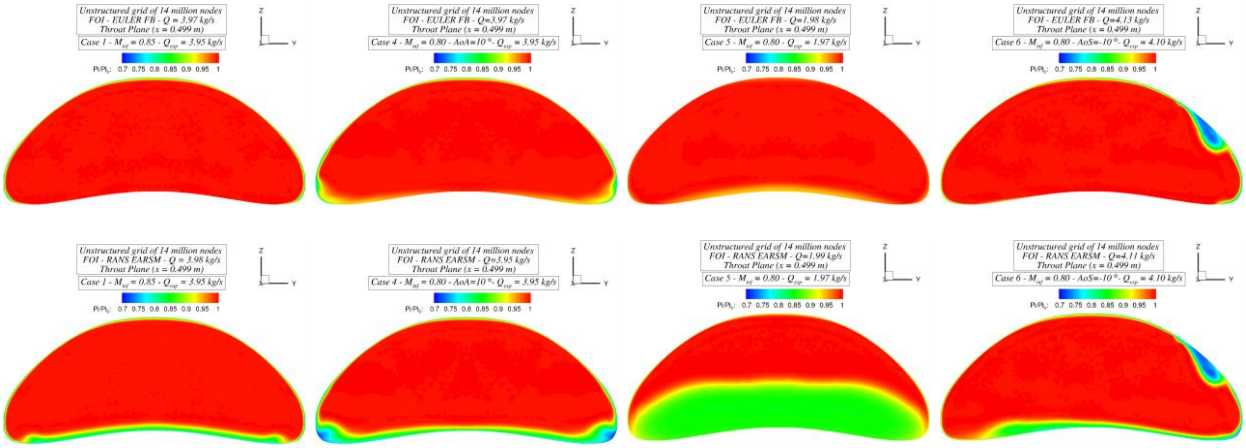

Figure 11: FOI results for test cases 1, 4, 5, and 6 (from left to right) on throat pressure recovery comparing without (top) and with (bottom) forebody boundary layer.

Case	Partner	Method	PR	DC60	CDI	RDI	SC60	$\dot{m}$ (kg/s)
1	FOI	RANS+Euler forebody	0.9625	0.6446	0.1304	0.0321	9.97	3.973
2	FOI	RANS+Euler forebody	0.9673	0.5947	0.1255	0.0306	8.50	9.601
3	FOI	RANS+Euler forebody	0.9623	0.6439	0.1307	0.0325	9.96	3.989
4	FOI	RANS+Euler forebody	0.9578	0.6497	0.1311	0.0363	10.72	3.968
5	FOI	RANS+Euler forebody	0.9870	0.6929	0.0278	0.0052	15.26	1.978
6	FOI	RANS+Euler forebody	0.9605	0.6240	0.1169	0.0285	10.11	4.130
7	FOI	RANS+Euler forebody	0.9640	0.6256	0.1260	0.0340	9.51	3.998
8	FOI	RANS+Euler forebody	0.9806	0.6298	0.0661	0.0153	10.29	3.060

Table 5: FOI results for diverted forebody boundary layer.

3.5 Intake Internal Flow Control

The effects of internal flow control were studied by FOI. Internal passive flow control was investigated by employing numerical models for the simulation of vortex generators (VG) in the intake duct. Simulations with active flow control devices in form of micro-jets were also carried out. Results were compared with experimental data for VG flow control cases.

The original FOI mesh was refined in the prescribed areas of the vortex generators to increase the grid densities and avoid too much dissipation. A total of 32 (64 for a full span mesh) VGs were applied in a two row configuration. The VGs were modelled as 3 mm high and 15 mm long flat plates. The micro-jets were modelled by a velocity inflow wall boundary condition applied at the same stations as the VGs.
Three methods were used to evaluate the flow control, RANS, URANS, and a hybrid RANS-LES (HYB0) method developed by Peng (see references [21] and [30]) at FOI. The steady state RANS calculations were done on a half span mesh whereas the time-dependent URANS and HYB0 were done on a full span mesh constructed by mirroring the half span mesh. A number of parameters were evaluated at the AIP and along the duct. The results for total pressures at the AIP are shown in **Figure 12**. Applying the VGs reduces the values for the distortion parameter DC60, but has little effect on pressure recovery. The HYB0 solution was closest to experimental DC60 values, but was still higher. The HYB0 was the only method to resolve the large vortical structures in the off-wall LES region

The jets were modelled with different inflow velocities, the lowest being 150 m/s and the highest 350 m/s, which correspond to supersonic jet inflow. With the jet flow control, it was possible to completely remove all flow separations, but the added mass flow from all jets is too high for a real practical design.
A more detailed description of the investigations on flow control is given in [9].

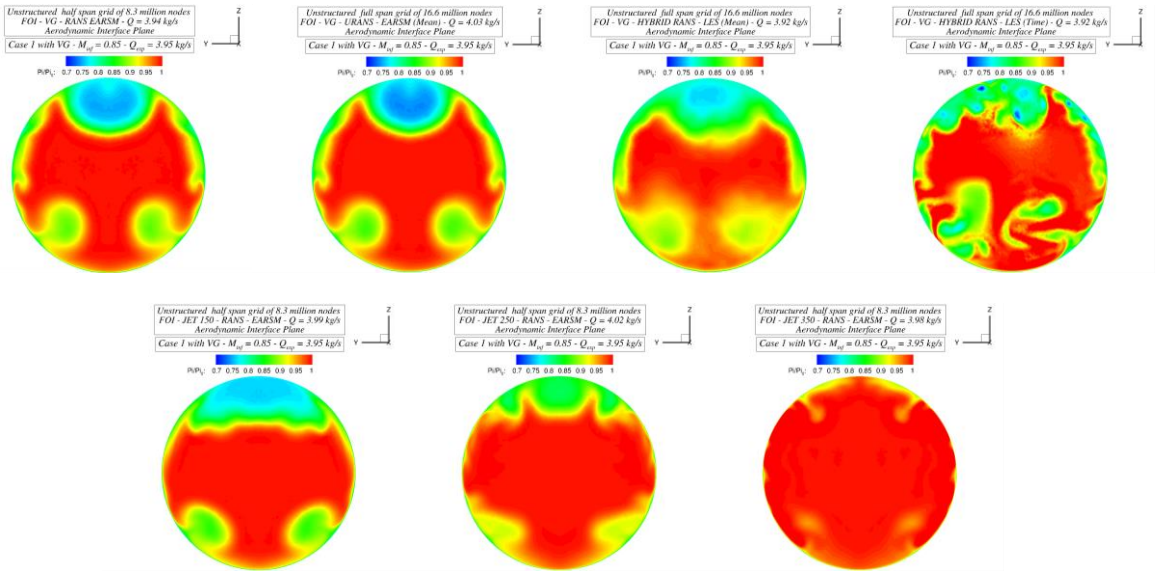

Figure 12: FOI results for total pressure recovery in the AIP applying flow control (top: vortex generators, bottom: micro-jets).

4 EFFECT OF BOUNDARY LAYER INGESTION INTO A GENERIC S-DUCT INTAKE: EXPERIMENTAL RESULTS FOR THE GENERIC INTAKE WIND TUNNEL MODEL

In addition to complex flows caused by serpentine intakes another aspect that may result in serious distortions and total pressure losses at the engine face is the ingestion of boundary layers. Intakes of unmanned aerial vehicles are often located on the upper surface of the fuselage at a somewhat rearward position. Diverters are usually not applied since such devices significantly contribute to high radar cross sections of the aircraft. The effect of ingesting the boundary layer formed on the wetted surface ahead of the intake is twofold. On the one hand it may increase the aerodynamic efficiency of the aircraft [31, 32], but on the other hand, the thickness of the ingested boundary layer has a most detrimental influence on the performance of the intake [33].

In order to study more closely the effect of ingested boundary layers on the performance of S-duct intakes, an experimental test setup was designed by DLR. The test setup allows for changing Mach and Reynolds numbers as well as boundary layer thickness and mass flux through an intake, independently of each other (see **Figure 13**). The geometry of the intake was defined analytically and is based on a superellipse with varying coefficients, thus realizing a nearly rectangular entry area and a circular area at the AIP. Downstream of the AIP, the diffuser is continued with a straight exhaust duct. In order to form a well-defined boundary layer ahead of the intake, the model is arranged on a flat plate at a defined distance from the leading edge. The length of the plate can be changed. In this manner the height of the boundary layer was varied with all other parameters remaining fixed.

For the measurements, the flat plate and the contours of the intake were equipped with static pressure orifices. At several positions also the time dependence of the pressure was measured. At the aerodynamic interface plane, a rotatable rake with six arms equipped with static Pitot probes as well as piezoelectric sensors was positioned in order to record the pressure distribution. Figure 13 shows the wind tunnel model and the rake viewed through the exhaust duct. Model and plate were mounted in the test section of the cryogenic blow-down tunnel DNW-KRG of the German-Dutch Wind Tunnels (DNW). The test section of the DNW-KRG is equipped with adaptive upper and lower walls. The mass flux through the intake was adjusted by positioning the adaptive walls at the end of the test section so that the pressure is locally reduced, thus imposing a pressure difference between the entry area of the intake and the exit of the exhaust duct. A particular feature of the cryogenic blow-down tunnel DNW-KRG is that, at a constant Mach number, the Reynolds number can be changed within wide bounds, both by pressurizing the tunnel and by reducing the temperature.

The experimental setup outlined in the preceding paragraph has been used to evaluate the combined effects of boundary layer ingestion and an S-duct diffuser on total pressure recovery and distortion at the engine face in a parametric study. Mach number, Reynolds number, mass flux, and boundary layer thickness have been varied. The performance of the intake is measured in terms of the total pressure loss in the AIP and of the distortion descriptor DC60 as defined in [28]. As an example, the influence of an ingested boundary layer and the mass flux on the conditions at the AIP is considered in **Figure 14**, where the total pressure distribution in the AIP is compared for a case with a small ($\delta/h = 0.12$) and large ($\delta/h = 0.39$) value of the thickness δ of the ingested boundary layer (scaled by the height h of the intake entry area) for the non-dimensional inverse air mass flow ratios ($\mu = Ac/Ao$) of $\mu \approx 0.81$ and $\mu \approx 1.04$ at otherwise same conditions ($M = 0.50$, $Re = 30 \cdot 106\ m^{-1}$). As can be seen, for both values of the inverse flow ratio the increase in boundary layer thickness results in an impairment of the pressure distribution in the AIP with the increased losses in total pressure in the lower part of the AIP hinting an intensified region of separated flow in the lower part of the intake.

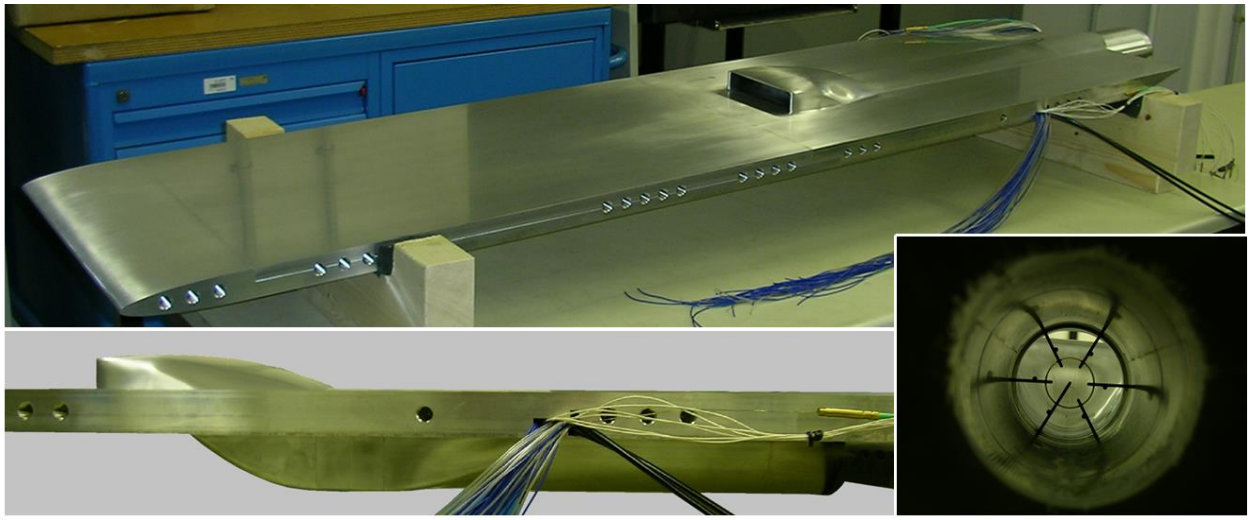

Figure 13: DLR intake wind tunnel model with flat plate for parametric study in the DNW-KRG, Göttingen (top: slanted view, bottom left: side view) and view from the rear exit of the exhaust pipe towards the measuring rake (bottom right).

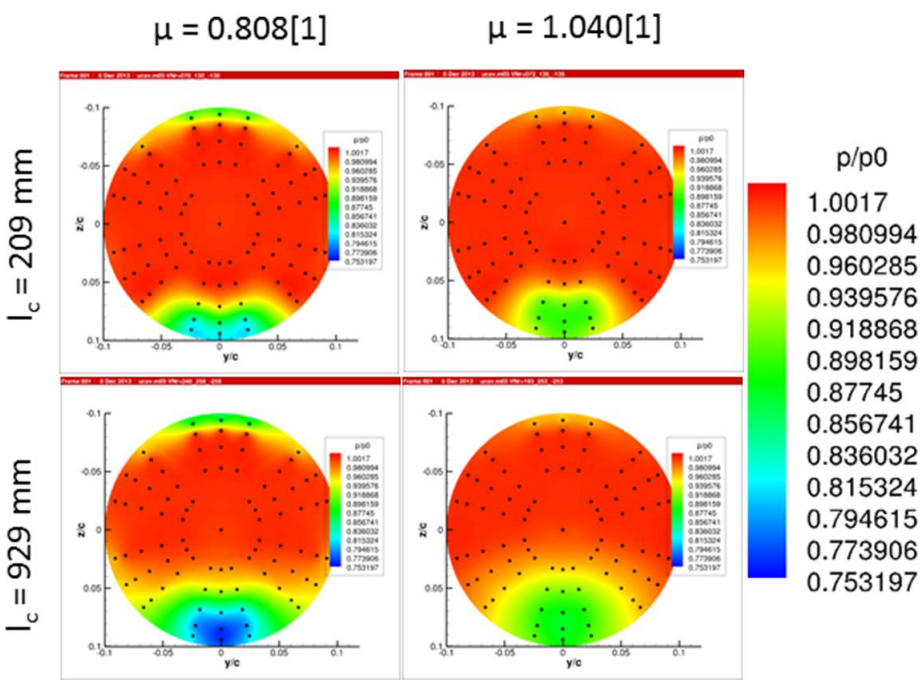

Figure 14: Total pressure distribution in the AIP of the wind tunnel model for two different boundary layer thicknesses: δ/h = 0.12 (top), δ/h = 0.39 (bottom), and two different inverse flow ratios: μ ≈ 0.81 (left) and μ ≈ 1.04 (right), (M = 0.50, Re = $30 \cdot 10^6$ m^{-1}).

The corresponding values of the distortion coefficient are DC60 = 0.24 and DC60 = 0.39 (μ ≈ 0.81) and DC60 = 0.34 and DC60 = 0.47 (μ ≈ 1.04), respectively. As can be seen, not only the boundary layer thickness but also the mass flux is of great importance. Above a critical mass flux (i.e., below the corresponding inverse flow ratio) whose value depends on the other parameters, the DC60 value was observed to increase markedly. This increase is likely connected with the occurrence of supersonic regions in the intake. A detailed description of the results is provided in [11].

5 CONCLUSIONS

The aerodynamic integration of serpentine diverterless intakes into low-observable unmanned aerial vehicles is a challenging task due to increased aerodynamic complexity. In order to support innovative design solutions unsteady flow phenomena of subsonic S-shaped air intakes were investigated by the Aerodynamics Action Group AD/AG-46 "Highly Integrated Subsonic Air Intakes" of the Group for Aeronautical Research and Technology in EURope (GARTEUR). In this paper a general overview of all investigations performed in the frame of GARTEUR AD/AG-46 was provided.

RANS, URANS, and DES computations were performed for the EIKON UAV configuration, which was designed and wind tunnel tested at FOI in Sweden, and the results were compared with data from T1500 wind tunnel experiments. The unsteady character of the intake flow field was clearly revealed by the CFD computations. Instantaneous and time-averaged results show low total pressure regions at the top and bottom of the intake duct with varying shapes, different sizes, and deviating intensities. The time evolutions of radial and circumferential distortion coefficients at the aerodynamic interface plane (AIP) very well demonstrate the highly turbulent flow in the separated region downstream of the S-duct. Flow field data from the computations describe effects related to Mach number, Reynolds number, angle of attack, angle of sideslip, and engine air mass flow. To accompany the design process of highly integrated subsonic air intakes, the prediction of instantaneous flow field parameters proved to be advantageous by applying a more advanced time-accurate method such as Detached Eddy Simulation (DES), especially with respect to dynamic intake distortion and thus engine/intake compatibility, even if capabilities still need to be enhanced in order to reach accuracy levels that are required for project-oriented applications. Present shortcomings related to accuracy, computing time, data gathering, and post-processing efforts will certainly be overcome in the near future, and industrial requirements will be met.

A numerical study on intake lip shaping was conducted. The drag and lift breakdown for the individual parts of the wind tunnel model as well as for the intake cowl allowed an improved assessment of the sources of the aerodynamic forces and an enhanced comparison of different cowl designs.

The impact of boundary layer ingestion versus boundary layer diversion was investigated in a computational trade-off study. Eliminating the boundary layer resulted in decreased total pressure losses and improved total pressure recoveries at the throat by approximately 2%, and distortion in the AIP could be reduced.

Internal passive flow control was investigated by employing numerical models for the simulation of vortex generators in the intake duct, and active flow control was studied by applying devices in form of micro-jets. Results were compared with experimental data. Applying the vortex generators reduces the values for the distortion parameter DC60, but has little effect on pressure recovery. The jets were modeled with different inflow velocities corresponding to supersonic jet inflow. With the jet flow active control, it was possible to completely remove all flow separations in the serpentine duct, but the added mass flow from all jets turned out to be too high for a current practical design.

Experiments with a generic high aspect ratio diverterless intake model were performed in the cryogenic blowdown wind tunnel DNW-KRG at DLR in Göttingen with the goal of contributing to a better understanding and correlation of installed performance predictions for highly integrated innovative intake designs. In a parametric study the combined effects of boundary layer ingestion and an S-shaped intake diffuser on total pressure recovery and distortion at the engine face were investigated as a function of Mach number, Reynolds number, boundary layer thickness, and intake mass flow ratio.

ACKNOWLEDGMENTS

The authors gratefully acknowledge the approval of the GARTEUR Council to publish the work of the Aerodynamics Action Group AD/AG-46 at the CEAS 2015 Conference.

Special thanks from all authors go to FOI for the provision of the EIKON UAV wind tunnel model geometry and for the experimental results from T1500 wind tunnel tests. Tools for the evaluation of the distortion parameters from the computational data were provided by AIRBUS Defence and Space Spain, which is gratefully acknowledged.

The authors greatly appreciate the support of their colleagues Kaare Sørensen, Dieter M. Schmitz, Bartholomäus Bichler at AIRBUS Defence and Space Germany, Sébastien Deck at ONERA, Björn Jonsson at the Swedish Defence Material Administration FMV, Stefan Wallin, Shia-Hui Peng, Adam Jirásek at FOI, and Stefan Koch at DLR.

Regarding communication, GARTEUR regularly presents its organization, provides the latest achievements obtained through its activities and outlines its orientations [34, 35, 36].

REFERENCES

[1] Delot, A.-L. and Scharnhorst, R. K., "A Comparison of Several CFD Codes with Experimental Data in a Diffusing S-Duct," AIAA-2013-3796, 49th AIAA/ASME/SAE/ASEE Joint Propulsion Conference, 14-17 July 2013, San Jose, CA, USA, with results of the first AIAA "Propulsion Aerodynamics Workshop," sponsored by the Air Breathing Propulsion System Integration Technical Committee, held on July 29, 2012 at the 48th AIAA Joint Propulsion Conference in Atlanta, Georgia.

[2] Mace, J., Lakebrink, M., Mani, M., and Steenken, W., "Computational Simulation of Dynamic Total-Pressure Distortion in an S-Diffuser," AIAA Paper 2012-3999, August 2012.

[3] Vuillerme, A-L., Deck, S., and Chevrier, R., "Numerical Simulations of the Flow Inside an S-shaped Intake Diffuser," European Conference for Aerospace Sciences (EUCASS), Session 2.4 "CFD Simulation I", Moscow, Russia, 4-7 July 2005.

[4] Spalart, P. R., Deck, S., Shur, M. L., Squires, K. D., Strelets, M. K., and Travin, A., "A New Version of Detached-Eddy Simulation, Resistant to Ambiguous Grid Densities," Theoretical and Computational Fluid Dynamics, 20, 181-195, 2006.

[5] Consigny, H., Vasseur, O., and Delot, A.-L., "An Overview of the Group for Aeronautical Research and Technology in EURope (GARTEUR)," AIAA-2014-0370, AIAA Science and Technology Forum and Exposition, 13-17 January 2014, National Harbor, MD, USA.

[6] Berens, T. M., Delot, A.-L., Tormalm, M. H., Ruiz-Calavera, L.-P., Funes-Sebastian, D.-E., Rein, M., Säterskog, M., Ceresola, N., and Zurawski, L., "Highly Integrated Subsonic Air Intakes," Group for Aeronautical Research and Technology in EURope (GARTEUR), AD/AG-46 Final Report, February 2014, to be published on GARTEUR Website http://www.garteur.org.

[7] Berens, T. M., Delot, A.-L., Tormalm, M. H., Ruiz-Calavera, L.-P., Funes-Sebastian, D.-E., Rein, M., Säterskog, M., Ceresola, N. and Zurawski, L., "Numerical and Experimental Investigations on Highly Integrated Subsonic Air Intakes," AIAA-2014-0722, AIAA Science and Technology Forum and Exposition, 13-17 January 2014, National Harbor, MD, USA.

[8] Delot, A.-L., Berens, T. M., Tormalm, M. H., Säterskog, M., and Ceresola, N., "DES Computations for a Subsonic UAV Configuration with a Highly Integrated S-Shaped Intake Duct," AIAA-2014-0723, AIAA Science and Technology Forum and Exposition, 13-17 January 2014, National Harbor, MD, USA.

[9] Tormalm, M., "Flow Control Using Vortex Generators or Micro-Jets Applied in a UCAV Intake," AIAA-2014-0724, AIAA Science and Technology Forum and Exposition, 13-17 January 2014, National Harbor, MD, USA.

[10] Funes-Sebastian, D.-E. and Ruiz-Calavera, L.-P., "Numerical Simulations of Wind Tunnel Effects on Intake Flow of a UAV Configuration," AIAA-2014-0372, AIAA Science and Technology Forum and Exposition, 13-17 January 2014, National Harbor, MD, USA.

[11] Rein, M., Koch, S., and Ruetten, M., "Experimental and Numerical Investigations on the Influence of Ingesting Boundary Layers into a Diverterless S-Duct Intake," AIAA-2014-0373, AIAA Science and Technology Forum and Exposition, 13-17 January 2014, National Harbor, MD, USA.

[12] Berens, T. M., Delot, A.-L., Chevalier, M., and Van Muijden, J., "Numerical Simulations for High Offset Intake Diffuser Flows," AIAA-2014-0371, AIAA Science and Technology Forum and Exposition, 13-17 January 2014, National Harbor, MD, USA.

[13] Berens, T. M., Delot, A.-L., Chevalier, M., Van Muijden, J., Waaijer, R. A., and Tattersall, P., "Application of CFD to High Offset Intake Diffusers," Group for Aeronautical Research and Technology in EURope (GARTEUR), AD/AG-43 Final Report, GARTEUR TP–173, Oct. 2012, to be published on Website http://www.garteur.org.

[14] Chevalier, M., & Peng, S.-H., "Detached Eddy Simulation of Turbulent Flow in a Highly Offset Intake Diffuser," in S.-H. Peng & W. Haase (Ed.), 2007 Symposium of Hybrid RANS-LES Methods (pp. 111-121), Springer-Verlag Berlin Heidelberg, 2010.

[15] Tormalm, M., "Propulsion Integration Project, Design and analysis of compact UAV ducts", FOI-R--2019--SE, ISSN 1650-1942, www.foi.se, June 2006.

[16] Johansson, M., "FoT25 2003-2005, Propulsion Integration, Final Report", FOI-R--2017--SE, ISSN 1650-1942, www.foi.se, June 2006.

[17] Samuelsson, I., "Test of the Effect of Vortex Generators in the Diffuser Duct of an UCAV Air Inlet (Forebody Model of Eikon) in FOI Transonic Wind Tunne3l T1500", FOI-R--2038--SE, ISSN 1650-1942, September 2006.

[18] Eliasson, P., "Edge, a Navier-Stokes solver for unstructured grids", Proc. To Finite Volumes for Complex Applications III, ISBN 1 9039 9634 1, pp.527-534, 2002.

[19] Wallin, S. and Johansson, A. V., "An explicit algebraic Reynolds stress model of incompressible and compressible flows", J. Fluid Mech., Vol. 403, pp. 89-132, 2000.

[20] Menter F. R., "Two-equation eddy-viscosity turbulence models for engineering applications", AIAA Journal, 32:1598–1605, 1994.

[21] Peng, S.-H., "Algebraic Hybrid RANS-LES Modelling Applied to Incompressible and Compressible Turbulent Flows". AIAA-Paper 2006-3910.

[22] Schwamborn, D., Gerhold, T., and Kessler, K., "DLR-TAU Code – an Overview," Proceedings of the 1st ONERA/DLR Aerospace Symposium, Paris, France, 1999.

[23] ANSYS-CFX Theory Guide.

[24] Deck, S., "Zonal-Detached-Eddy Simulation of the Flow Around a High-Lift Configuration," AIAA Journal, 43(11): 2372–2384, November 2005.

[25] Deck, S., "Recent Improvements in the Zonal Detached Eddy Simulation (ZDES) formulation," Theoretical and computational fluid Dynamics (2012), Vol. 26 (6), pp 523–550. DOI 10.1007/s00162-011-0240-z.

[26] Deck S., Laraufie R., "Numerical investigation of the flow dynamics past a three-element aerofoil," J. Fluid Mech. (2013), Vol. 732, pp. 401-444, doi:10.1017/jfm.2013.363, 2013.

[27] Deck, S. & Thorigny, P., "Unsteadiness of an axisymmetric separating-reattaching flow: numerical investigation," Phys. Fluids 19, 065103, 2007.

[28] Seddon, J. and Goldsmith, E. L., "Intake Aerodynamics," Second edition, AIAA Education Series, 1999.

[29] SAE, ARP1420, Rev. B, "Gas Turbine Engine Inlet Flow Distortion Guidelines", 2002.

[30] Peng, S.-H., "Hybrid RANS-LES modelling based on zero- and one-equation models for turbulent flow simulation", In Proceedings of the 4th International Symposium on Turbulence and Shear Flow Phenomena, Volume 3, pages 1159-1164, 2005.

[31] Betz, A., "Einführung in die Theorie der Strömungsmaschinen," Verlag G. Braun, Karlsruhe, pp 204-207, 1959.

[32] Martin, P. G., "Challenges in the design of air intakes for subsonic UAVs," Proc. RAeS Aerospace Aerodynamics Research Conference, 10-12 June 2003, London, 2003, pp. 23.1-6, 2003.

[33] Godard, J.-L., "Semi-Buried Engine Installation: the Nacre Project Experience", 27th Int. Congress of the Aeronautical Sciences (ICAS), 2010.

[34] Consigny, H., Vasseur, O., and Delot, A.-L., "Overall View of the European Collaboration in Aeronautics Research within GARTEUR," 5th CEAS Air & Space Conference, paper no. 40, 7-11 Sept. 2015, Delft University of Technology (The Netherlands) (submitted for publication).

[35] Dieterich, O. and Pavel, M.D., "Rotorcraft-Pilot Coupling Research in Europe: A Success Story in Collaboration," 5th CEAS Air & Space Conference, paper no. 58, 7-11 Sept. 2015, Delft University of Technology (The Netherlands) (submitted for publication).

[36] Riccio, A., "GARTEUR Structures & Materials Action Group 32 – A European Research Project on Damage Growth In Aerospace Composite Structures," 5th CEAS Air & Space Conference, paper no. 78, 7-11 Sept. 2015, Delft University of Technology (The Netherlands) (submitted for publication).